

Atomic magnetometer with microfabricated vapor cells based on coherent population trapping

Xiaojie Li(李晓杰), Yue Shi(史越), Hongbo Xue(薛洪波), Yong Ruan(阮勇), and Yanying Feng(冯焱颖)

Citation: Chin. Phys. B, 2021, 30 (**3**): 030701. DOI: 10.1088/1674-1056/abc2b9
Journal homepage: http://cpb.iphy.ac.cn; http://iopscience.iop.org/cpb

What follows is a list of articles you may be interested in

Miniature quad-channel spin-exchange relaxation-free magnetometer for magnetoencephalography

Jian-Jun Li(李建军), Peng-Cheng Du(杜鹏程), Ji-Qing Fu(伏吉庆), Xu-Tong Wang(王旭桐), Qing Zhou(周庆), Ru-Quan Wang(王如泉)

Chin. Phys. B, 2019, 28 (**4**): 040703. DOI: 10.1088/1674-1056/28/4/040703

A dual-axis, high-sensitivity atomic magnetometer

Rujie Li(李茹杰), Wei Quan(全伟), Wenfeng Fan(范文峰), Li Xing(邢力), Zhuo Wang(王卓), Yueyang Zhai(翟跃阳), Jiancheng Fang(房建成)

Chin. Phys. B, 2017, 26 (**12**): 120702. DOI: 10.1088/1674-1056/26/12/120702

Spin dynamics of magnetic resonance with parametric modulation in a potassium vapor cell

Rui Zhang(张锐), Zhi-Guo Wang(汪之国), Xiang Peng(彭翔), Wen-Hao Li(黎文浩), Song-Jian Li(李松健), Hong Guo(郭弘)

Chin. Phys. B, 2017, 26 (**3**): 030701. DOI: 10.1088/1674-1056/26/3/030701

In-situ measurement of magnetic field gradient in a magnetic shield by a spin-exchange relaxation-free magnetometer

Fang Jian-Cheng, Wang Tao, Zhang Hong, Li Yang, Cai Hong-Wei

Chin. Phys. B, 2015, 24 (**6**): 060702. DOI: 10.1088/1674-1056/24/6/060702

A laser pump-re-pump atomic magnetometer

Yang Ai-Lin, Yang Guo-Qing, Cai Xun-Ming, Xu Yun-Fei, Lin Qiang

Chin. Phys. B, 2013, 22 (**12**): 120702. DOI: 10.1088/1674-1056/22/12/120702

Atomic magnetometer with microfabricated vapor cells based on coherent population trapping*

Xiaojie Li(李晓杰)[1,2,3], Yue Shi(史越)[1,2,3], Hongbo Xue(薛洪波)[4], Yong Ruan(阮勇)[1,2,3,5,†], and Yanying Feng(冯焱颖)[1,2,3,‡]

[1] *State Key Laboratory of Precision Measurement Technology and Instrument, Tsinghua University, Beijing* 100084, *China*
[2] *Key Laboratory of Photonic Control Technology (Ministry of Education), Tsinghua University, Beijing* 100084, *China*
[3] *Department of Precision Instrument, Tsinghua University, Beijing* 100084, *China*
[4] *State Key Laboratory of Space Weather, National Space Science Center, Chinese Academy of Sciences, Beijing* 100190, *China*
[5] *MEMS Institute of Zibo National High-tech Industrial Development Zone, Zibo* 255086, *China*

(Received 19 August 2020; revised manuscript received 30 September 2020; accepted manuscript online 20 October 2020)

An atomic magnetometer based on coherent population trapping (CPT) resonances in microfabricated vapor cells is demonstrated. Fabricated by the micro-electro-mechanical-system (MEMS) technology, the cells are filled with Rb and Ne at a controlled pressure. An experimental apparatus is built for characterizing properties of microfabricated vapor cells via the CPT effects. The typical CPT linewidth is measured to be about 3 kHz (1.46 kHz with approximately zero laser intensity) for the rubidium D1 line at about 90 °C. The effects of pressure, temperature and laser intensity on CPT linewidth are studied experimentally. A closed-loop atomic magnetometer is finally finished with a sensitivity of 210.5 pT/Hz$^{1/2}$ at 1 Hz bandwidth. This work paves the way for developing an integrated chip-scale atomic magnetometer in the future.

Keywords: atomic magnetometer, MEMS, vapor cell, coherent population trapping

PACS: 07.55.Ge, 85.85.+j, 76.70.Hb, 42.50.Gy **DOI:** 10.1088/1674-1056/abc2b9

1. Introduction

Atomic sensors have been widely served as precision measurement sensors in various applications, such as atomic clocks, magnetometers, and gyroscopes.[1,2] Measuring magnetic fields enable a characterization for many significant physical phenomena in many fields of science, including physics, geology and biology.[3–5] Traditionally, magnetometry with a sensitivity in the fT range depends on low-temperature superconducting quantum interference device (SQUID) magnetometers.[6] However, SQUIDs need expensive liquid helium maintained in a superconducting state, resulting in huge size and high maintenance costs. With no requirement for cryogenic equipment, atomic magnetometers have been recognized as a potential candidate for SQUIDs in the applications needing ultra-low noise magnetic sensors like biomagnetic measurement.[7–10]

On the other hand, the potential of atomic magnetometers in chip-scaled integration and wafer-level fabrication endows them to have advantages in field applications and enlarges the applying scope of ultra-sensitive magnetometers. Recent progresses of MEMS technology on fabricating atomic sensors, especially microfabricated vapor cell, have leaded to demonstrations of chip-scaled atomic magnetometers.[11–14] A representative chip-scale atomic magnetometer has been constructed with a sensitivity of 50 pT/Hz$^{1/2}$ at 10 Hz by Schwindt *et al.* in 2004.[12] With the advantages of size and power consumption, chip-scale atomic magnetometers can maintain performances in terms of stability and sensitivity.[15–17]

In this work, an atomic magnetometer based on the CPT effects in microfabricated vapor cells is demonstrated. These cells were designed and fabricated with wafer-level fabrication technology in our previous works.[18–20] The performance of these microfabricated vapor cells is characterized and the potential as a core component for a chip-scale atomic magnetometer is evaluated. A closed-loop atomic magnetometer based on the microfabricated vapor cell is built and measured.

2. Theory on CPT

CPT was first demonstrated by Alzetta *et al.* when they detected dark lines in the fluorescence emitted by a beam of sodium atoms in 1976.[21] The phenomenon is induced by the interaction between atom and two phase-coherent light fields $\boldsymbol{E}_1$ and $\boldsymbol{E}_2$ at frequencies ω_1 and ω_2, respectively. The three-level atomic levels and light fields, forming a Λ configuration, are shown in Fig. 1(a). When the beat frequency between the two resonant laser fields exactly equals the atomic ground state hyperfine splitting Δ, i.e., $\omega_1 - \omega_2 = \Delta$, atoms are driven into

*Project supported by the National Natural Science Foundation of China (Grant No. 61473166).
†Corresponding author. E-mail: ruanyong@tsinghua.edu.cn
‡Corresponding author. E-mail: yyfeng@tsinghua.edu.cn
© 2021 Chinese Physical Society and IOP Publishing Ltd

a coherent superposition state of the two ground state levels and absorb no photons anymore, called the dark state.

Before interacting with light, the atomic population is equally distributed between two low energy states, $|b\rangle$ and $|c\rangle$. During the interaction with light, the atoms are excited to state $|a\rangle$, and then spontaneously decay either into the dark state or into its orthogonal counterpart, the bright state. The atoms in the dark state do not interact with the laser fields and remain in this state, while the atoms in the bright state interact until all atoms end up in the dark state. After such a steady state is achieved, the atomic medium becomes transparent, because both resonant light fields propagate without any optical losses, which is called the coherent population trapping effect.[22]

The full width at half maximum (FWHM) of the CPT resonance line, shown as Lorentzian shape, reads[23,24]

$$\Delta\nu_{(\mathrm{FWHM})} = \frac{1}{\pi}\left(\gamma_2 + \frac{\omega_{\mathrm{R}}^2}{\Gamma^\star}\right), \tag{1}$$

where γ_2 is the hyperfine coherence relaxation rate, $\Gamma^\star$ the decay rate from the excited state or linewidth of the optical resonance, which increases with the buffer gas pressure, and ω_{R} the optical Rabi pulsation related to the laser intensity I.

As shown in Eq. (1), the CPT resonance linewidth increases linearly with laser intensity in a slope proportional to the inverse optical linewidth. The zero-intensity limit is only given by the ground state coherence. Because the spontaneous radiative decay between two hyperfine states of the same ground state is strictly forbidden, an atom in the dark state can maintain its coherence state until it interacts with its environment, such as atomic collisions with glass wall of a vapor cell. Filling a pressure of buffer gases in the cell can reduce the diffusive motion of atoms and makes it possible to preserve the ground state coherence, meaning the decrease of FWHM.

Based on the magnetic sensitivity of the CPT resonances in vapor cell (with buffer gas), an atomic magnetometer can be demonstrated with a high sensitivity. Figure 1(b) shows the schematic of light-induced two-photo transitions of D1 line of ^{87}Rb atom from $F_{\mathrm{g}} = 1, 2$ to $F_{\mathrm{e}} = 2$ in the case of σ–σ transition scheme. The two-photo transitions between two ground states $F_{\mathrm{g}} = 1, m_{\mathrm{F}} = -1/1$ with $F_{\mathrm{g}} = 2, m_{\mathrm{F}} = -1/1$ is affected by the Zeeman level splitting. Under weak magnetic conditions, the energy between the ground state Zeeman level with the $m_{\mathrm{F}} = n$ can be written as

$$\nu_{n-n} = \nu_{0-0} + 2n\gamma B, \tag{2}$$

where ν_{0-0} is the energy of atomic ground state hyperfine splitting, γ the gyromagnetic ratio, and B the magnetic field.

As shown in Eq. (2), the value of ν_{n-n} is proportional to magnetic field magnitude B. The 0–0 central resonance signal is called the clock transition, meanwhile the -1–-1 and 1–1 signals are magnetic-sensitive resonance transition. By decreasing the FWHM of these CPT resonance peaks, the resolution of frequency measurements of the hyperfine or Zeeman resonance can be improved and leads to more sensitive magnetic field measurement.

3. Experimental setup

Figure 1(c) shows the schematic of the experimental apparatus. A 795 nm external cavity diode laser (ECDL, DL pro, TOPTICA) is locked to resonance transition of $F_{\mathrm{g}} = 1$ to $F_{\mathrm{e}} = 2$ of ^{87}Rb D1 line, with Zeeman modulation frequency stabilization technology. After coupled into an optical fiber via a fiber coupler, the light is modulated by a fiber electro-optic modulator (FEOM,PM-0S5-10-PFA-PFA, EOSPACE) driven at 6.834 GHz by an RF microwave source (N5181A, AGILENT), and the phase-coherent light for the CPT resonance is formed with two different frequencies. A linear polarizer and quarter wave plate are used to generate the circular polarization light for the σ–σ transition scheme. Then the light passes the microfabricated vapor cell placed in a five-layer magnetic shields, and is detected by a photodiode (PDA36A, THORLABS). The resonance error signal is acquired with a lock-in amplifier (LIA, LIA-MVD-200-H, FEMTO). A signal generator (33522B, KEYSIGHT) provides the reference signal for the microwave generator and LIA loop. The CPT signal from LIA is acquired by a data acquisition board (DAQ) for closed-loop control. Finally, the system is closed-loop locked by a PID error compensation control.

Microfabricated Rb vapor cells are fabricated using two-step glass-silicon anodic bonding techniques and dispenser pills of SAES Getters, containing both ^{85}Rb and ^{87}Rb.[20] As shown in Fig. 1(d), these cells have a dual-cavity structure with an optical cavity and a reaction cavity. The square reaction cavity contains the dispenser pill and act as a reservoir of Rb atoms, while the cylindrical one with radius size of about $r = 2.5$ mm acts as the optical cavity for CPT detection. The two cavities are connected via a micro channel. Two cells are used in the experiments, labeled as 1 and 2, respectively. The pressure of buffer gas in cell 1 is about 8.9 kPa in 90 °C, while that of cell 2 is about 4.0 kPa.

The microfabricated vapor cell is placed in the center of the magnetic shields and magnetic coils, which provides a bias static magnetic field along the direction of light. A heating system including intermittent electrical heating and high frequency electrical heating is utilized to heat the cells up to about 90 °C. The heating current is turned off while collecting the data of CPT signal, thus the interference caused by electric heating can be negligible.

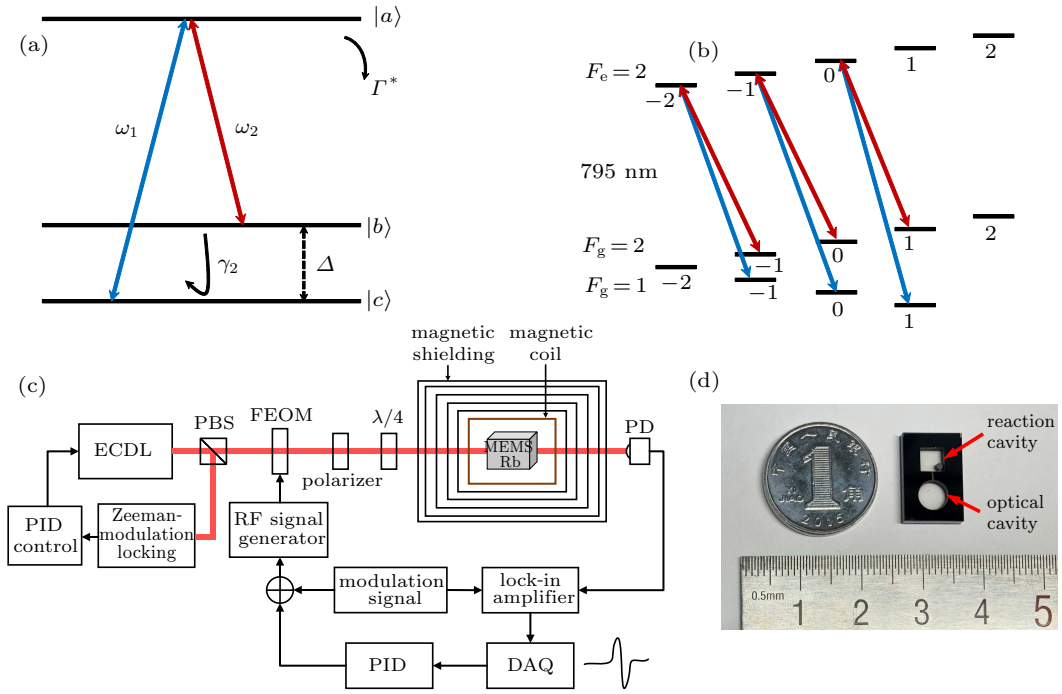


Fig. 1. Schematic diagrams of the theory and apparatus. (a) The interaction of light with three-level atom in a Λ configuration. (b) Light-induced two-photo transitions of D1 line of ^{87}Rb atoms in the case of σ–σ transition scheme. (c) CPT resonance measurement apparatus in the case of σ–σ transition scheme. ECDL: external cavity diode laser; PBS: polarization beam splitter; FEOM: fiber electro-optic modulator; Polarizer: linear polarizer; $\lambda/4$: quarter wave plate; PD: photodiode. (d) The experimental microfabricated vapor cells with the radius size of optical cavity about 2.5 mm.

4. Results and discussion

A typical experimental absorption spectrum obtained in the cells operating in about 90 °C is shown in Fig. 2, where four peaks correspond to four atomic transitions of natural abundance rubidium. The buffer gas in the cells broadens the absorption spectrum because of the collision between Rb atoms and Ne atoms. With the increase of the buffer gas pressure, the absorption line broadening gradually increases, as shown in Fig. 2. Due to the higher pressure of buffer gases, the absorption peaks of cell 1 have wider line width than those of cell 2, and even a peak of ^{87}Rb overlapped with the peak of ^{85}Rb nearby in cell 1.

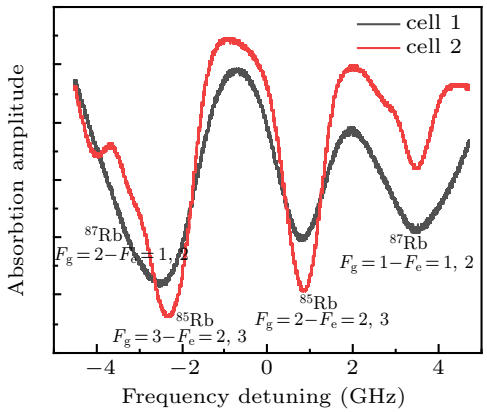


Fig. 2. The experimental absorption spectrum obtained in the microfabricated vapor cells 1 and 2 operating in about 90 °C. The absorption peaks are broadened clearly.

To obtain the CPT resonance, the laser is modulated by applying 6.834 GHz high-frequency signal from the RF microwave source to the FEOM. The CPT spectrum is acquired by sweeping the frequency. In the presence of a bias magnetic field, the CPT spectrum will have three separated Zeeman resonance peaks. The frequency of RF microwave source is modulated by a sine signal in addition to its frequency sweep and a lock-in amplifier is used to get the corresponding error signal of the CPT line. Experimentally, Fig. 3 shows the Zeeman spectrum and its corresponding error signal in cell 2.

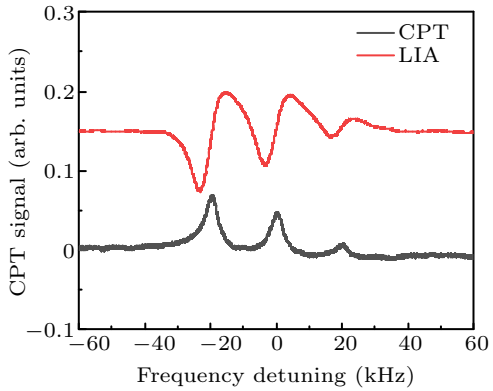


Fig. 3. The typical experimental Zeeman spectrum and its corresponding error signal obtained in the Rb-Ne microfabricated vapor cell 2. The CPT 0–0 resonance linewidth is about 4.2 kHz.

The laser intensity is 4.1 μW with the beam waist size approximately covering the optical cavity of cell. The static magnetic field B is about 1.4 μT, so the frequency shift of the 1–1 resonance with the 0–0 resonance is calculated to be about 20.3 kHz, which is matched with the results in Fig. 3. The CPT 0–0 resonance linewidth is about 4.2 kHz. The am-

plitude of −1−−1 resonance peak is higher than that of 1–1 resonance, due to optical pumping effect in the case of σ–σ transition scheme. It can be shown that the Ne buffer gas reduces the CPT line-width efficiently, compared with those of cells without buffer gas, which can be several hundreds of kHz correspondingly.

Figure 4 shows the effect of the cell temperature on the linewidth of the 0–0 resonance for the cells 1 and 2.

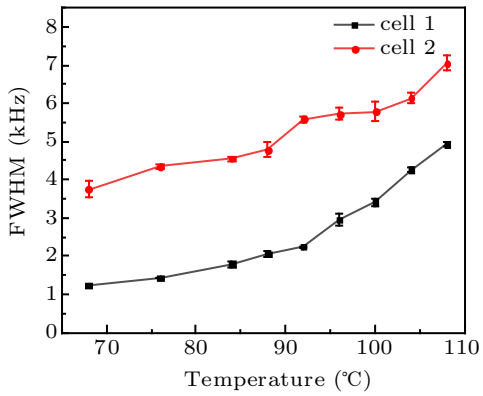


Fig. 4. The effect of the cell temperature on the linewidth of the 0–0 resonance for the cells 1 and 2. The CPT line widths are increased with the rising temperatures for both cells.

With the rising temperature, the CPT line widths increase for both cells. This is due to the increase of the total relaxation rate of the vapor cell when the atomic density and velocity increase with the temperature, and rubidium atoms collide with the cavity wall or other atoms more frequently. Owing to the higher buffer gas pressure in cell 1, the FWHM of cell 1 is smaller than that of cell 2 at the same temperature. There is not an optimal value for the effect of cell temperature on the CPT line width at the temperatures in our experiment. The CPT line widths increases with the rising temperature. However, the amplitude of the CPT signal has an optimization point around 90 °C. For optimizing the signal-to-noise ratio (SNR) of the CPT signal, the operation temperature of the cell in the atomic magnetometer is set to 90 °C.

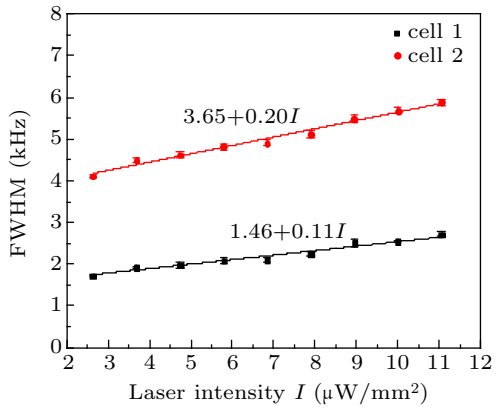


Fig. 5. The linewidth of CPT resonance versus the total laser intensity for two Rb–Ne microfabricated vapor cells. The CPT linewidth linearly increases with laser intensity due to power broadening.

The laser intensity of pump light can also broaden the linewidth of CPT resonance. Figure 5 shows the linewidth of CPT resonance versus the total laser intensity for these two Rb–Ne cells. According to Eq. (1), the CPT linewidth linearly increases with laser intensity due to power broadening. Fit functions of the linewidth-intensity dependence are $(3.65+0.20I)$ kHz and $(1.46+0.11I)$ kHz for the cells 1 and 2, respectively. The ultimate linewidth of cell 1 can reach 1.46 kHz with approximately zero laser intensity. The slope of the increase is lower for the cell 1 with higher buffer gas pressure, because the optical linewidth, $\Gamma^{\star}$, increases with the buffer gas pressure.

Frequency modulation (FM) mode is used in the RF signal source with modulation frequency at 2.5 kHz to enable phase-sensitive detection on the CPT resonance and obtain related error signal. Lock-in amplifier and PID control are used to compensate for the frequency error. When changing the magnetic field step by step, the resulting signal from the PID control in cell 1 is shown in Fig. 6, which has been converted into the corresponding magnetic field. The step interval of magnetic field changing is about 0.5 s, and the magnetic field density has been changed 95 nT in each step.

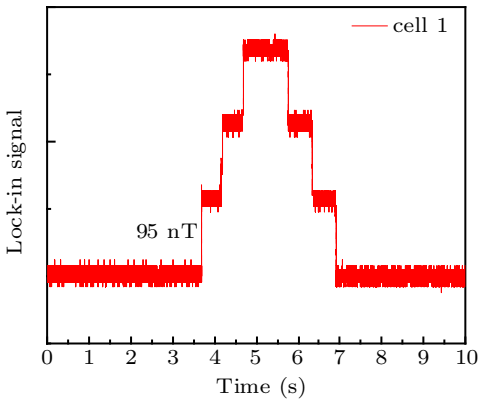


Fig. 6. The resulting signal from the lock-in amplifier in cell 1. The step interval of magnetic field changing is about 0.5 s with the magnetic field density changing 95 nT in each step.

With a collecting time of 200 s, the corresponding noise spectrum of the CPT signal is calculated, as shown in Fig. 7. The power frequency giving rise to the 50 Hz peak in the spectrum. The sensitivity of this magnetic sensor based on a microfabricated vapor cell is measured to be 210.5 pT/Hz$^{1/2}$ at 1 Hz bandwidth. Several possible sources of the noise in the magnetometer, such as fluctuations of the ambient field, laser intensity and temperature, vibrations of the detecting apparatus and electrical noise of the signal processing circuits, limit the sensitivity. The noise of the heating circuit cannot be ignored when collecting data for a long time. Further, the sensitivity of this atomic magnetometer can be improved by decreasing the noise of the circuits and optimizing the reaction coefficient of compensation system.

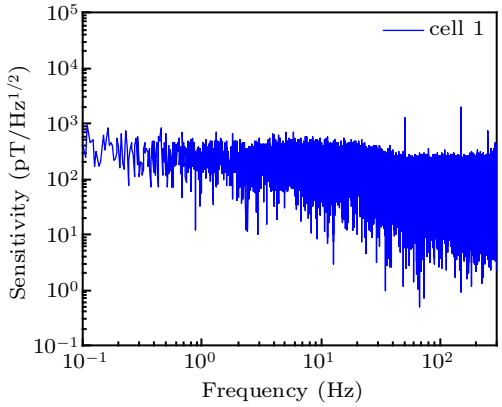


Fig. 7. The noise power spectrum density of the lock-in CPT signal of cell 1. The measured sensitivity of this magnetic sensor based on a microfabricated vapor cell is 210.5 pT/Hz$^{1/2}$ at 1 Hz bandwidth.

5. Conclusion

In summary, a closed-loop atomic magnetometer with a microfabricated vapor cell based on the CPT resonance has been demonstrated. The performance of the microfabricated vapor cell fabricated in a wafer level by the two-step glass-silicon anodic bonding techniques has been characterized experimentally. Effects of parameters like buffer gas pressure, temperature and laser intensity on the CPT resonance linewidth are studied. The typical CPT linewidth is about 3 kHz (1.46 kHz with approximately zero laser intensity) on the rubidium D1 line at about 90 °C. Finally, a closed-loop CPT magnetometer based on the microfabricated vapor cell is built and measured to be of a sensitivity of 210.5 pT/Hz$^{1/2}$ at 1 Hz bandwidth. These results proved that these microfabricated vapor cells can be served as a core component for a chip-scale atomic magnetometer. Future work will be focused on the development of an integrated chip-scale atomic magnetometer and the improvement of the sensitivity of the atomic magnetometer for biomedical applicaiton.

References

[1] Kitching J, Knappe S and Donley E A 2011 *IEEE Sens. J.* **11** 1749

[2] Kitching J, Donley E A, Knappe S, Hummon M, Dellis A T, Sherman J, Srinivasan K, Aksyuk V A, Li Q L, Westly D, Roxworthy B and Lal A 2016 *J. Phys. Conf. Ser.* **723** 012056

[3] Bison G, Wynands R and Weis A 2005 *J. Opt. Soc. Am. B* **22** 77

[4] Merrill R T, McElhinny M W and McFadden P L 1998 *The Magnetic Field of the Earth: Paleomagnetism, the Core, and the Deep Mantle* 3nd edn (San Diego: Academic Press) p. 19

[5] Budker D and Romalis M 2007 *Nat. Phys.* **3** 227

[6] Weinstock H 2012 *SQUID Sensors: Fundamentals, Fabrication and Applications* 2nd edn (Berlin: Springer Science+Business Media) p. 307

[7] Allred J C, Lyman R N, Kornack T W and Romalis M V 2002 *Phys. Rev. Lett.* **89** 130801

[8] Shah V, Knappe S, Schwindt P D D and Kitching J 2007 *Nat. Photonics* **1** 649

[9] Dang H B, Maloof A C and Romalis M V 2010 *Appl. Phys. Lett.* **97** 151110

[10] Li J J, Du P C, Fu J Q, Wang X T, Zhou Q and Wang R Q 2019 *Chin. Phys. B* **28** 040703

[11] Li S L, Xu J, Zhang Z Q, Zhao L B, Long L and Wu Y M 2014 *Chin. Phys. B* **23** 074302

[12] Schwindt P D D, Knappe S, Shah V, Hollberg L, Kitching J, Liew L and Moreland J 2004 *Appl. Phys. Lett.* **85** 6409

[13] Zhang Y J, Li Y C, Hu X W, Zhang L, Liu Z J, Zhang K F, Mou S H, Zhang S G and Yan S B 2019 *Chin. Opt. Lett.* **17** 040202

[14] Hasegawa M, Chutani R K, Gorecki C, Boudot R, Dziuban P, Giordano V, Clatot S and Mauri L 2011 *Sens. Actuator A* **167** 594

[15] Sander T H, Preusser J, Mhaskar R, Kitching J, Trahms L and Knappe S 2012 *Biomed. Opt. Express* **3** 981

[16] Knappe S, Schwindt P D D, Shah V, Hollberg L, Kitching J, Liew L and Moreland J 2005 *Opt. Express* **13** 1249

[17] Schwindt P D D, Lindseth B, Knappe S, Shah V, Kitching J and Liew L 2007 *Appl. Phys. Lett.* **90** 081102

[18] Han R Q, You Z, Zhang F and Ruan Y 2017 *Joint Conference of the European Frequency and Time Forum and IEEE International Frequency Control Symposium (EFTF/IFCS)*, July 9–13, 2017, Besancon, France, pp. 296–299

[19] Han R Q, You Z, Zhang F, Xue H B and Ruan Y 2018 *Micromachines* **9** 175

[20] Zhang F, Ruan Y, Feng Y Y and Han R Q 2018 *IEEE CSAA Guidance, Navigation and Control Conference (CGNCC)*, August 10–12, 2018, Xiamen, China, pp. 1–5

[21] Alzetta G, Gozzini A, Moi L and Orriols G 1976 *Nuov. Cim. B* **36** 5

[22] Belcher N, Mikhailov E E and Novikova I 2009 *Am. J. Phys.* **77** 988

[23] Vanier J 2005 *Appl. Phys. B* **81** 421

[24] Boudot R, Dziuban P, Hasegawa M, Chutani R K, Galliou S, Giordano V and Gorecki C 2011 *J. Appl. Phys.* **109** 014912